Acceleration of changes in global surface temperature after the Earth system has crossed a tipping point

Grégory Beaugrand[1*], Philip C. Reid[2], Alessandra Conversi[3]

[1]CNRS, Univ. Lille, Université de Lille, Université du Littoral Côte d'Opale, UMR 8187, Laboratoire d'Océanologie et de Géosciences, 62930 Wimereux, France

[2]The Marine Biological Association, The Laboratory, Citadel Hill, Plymouth, Devon PL1 2PB, UK

[3]CNR, ISMAR (Institute of Marine Sciences) Lerici, Forte Santa Teresa, Loc. Pozzuolo, 19032 Lerici, Italy

*Corresponding author: Gregory.beaugrand@univ-lille.fr

Orcid author 1: https://orcid.org/0000-0002-0712-5223

Orcid author 2; https://orcid.org/0000-0001-7728-6746

Orcid author 3: https://orcid.org/0000-0002-8566-8282

Supplementary Material

Text S1

Our simulated time series of global temperature

Our simulated time series of global temperatures were designed to mimic a specific series of events that may be observed in GSTA: the occurrence of a tipping point, followed by a critical transition (with a phase of acceleration and deceleration), and finally the establishment of a new regime (i.e. a dynamic equilibrium). The proposal of indicators that separate the tipping point from the critical transition is important because when the tipping point is crossed, changes become irreversible, whatever the level of autocorrelation or the value of the trend.

Our simulated time series had a trend, a cyclical and a year-to-year component. It is difficult to separate the tipping point from the critical transition and then to identify the different phases of the critical transition until the establishment of the new regime. The simulated time series aims to explain how we can attempt to separate these different events. To do so, we used a logistic function to simulate the critical transition (see the section "Modelling a critical transition" below). The cyclical component was simulated to reproduce the pseudo-cyclical variability (or the alternation of negative and positive natural short-term perturbations) observed in GSTA (see the section "Modelling a cycle" below). The year-to-year component was simulated to reproduce the high-frequency variability observed in GSTA (see the section "Modelling year-to-year variability" below).

We also mimic a reduction in the negative phases of the cycle (and cycle + year-to-year variability) to simulate a reduction in the strength of negative retroactions that we postulate may occur when the system approaches the tipping point (see the section "Altering the amplitude of cyclical/year-to-year variability" below).

Modelling a critical transition

To describe our framework, we use a logistic trend to model a critical transition. A logistic curve can simulate different critical transitions from quasi-instantaneous stepwise shifts to more gradual ones (Fig. S1)(Beaugrand et al. 2022):

$$x_{t+1} = x_t + r x_t \left(1 - \frac{x_t}{K}\right) \qquad \textbf{Equation S1}$$

With x_{t+1} and x_t the value of global temperature (or GSTA) at time t+1 and t, respectively, r the rapidity with which global temperature adjusts to new conditions (e.g. greenhouse gas radiative forcing) and K global temperature at the new dynamic equilibrium (or state). Three parameters can influence the shape of this logistic curve: x_1 (global temperature at t=1), r and K (Fig. S1)(Beaugrand et al. 2022).

The position of the states, the tipping point and the critical transition are indicated in Fig. S1a. A state is a dynamic equilibrium, also called basin of attraction (Kump et al. 2004). A state is characterised by an absence of a permanent temporal autocorrelation. The tipping point, more difficult to locate precisely, should be in the zone where the rise in global temperature starts to be perceptible. It should also be located before the acceleration phase that leads to the inflection point of the curve (i.e. K/2). The critical transition is more precisely located because it is located around the inflection point of the logistic curve. In this model, the speed and duration of the critical transition depends upon r and to a lesser extent K (Fig. S1b).

Because a critical transition can exhibit very different shapes, which can alter our perception of the phenomenon, we looked for the shape that best fitted long-term changes in GSTA (1880-2022). To do so, we generated a total of 63105 logistic curves and retained the 10 curves that best fitted long-

term changes in GSTA. We used the following combinations: the values of x_1 had the following values: 0.0001, 0.001, 0.05, 0.01, 0.025, 0.1, and 1 (a total of 7 values); r had the following values: 0.0001, and from 0.001 to 0.6 every step of 0.001 (a total of 601 values); the values of K ranged from 1 to 15°C (a total of 15 values). The total number of combinations was therefore 7 x 601 x 15 = 63,105. The best fit was chosen by calculating the sum of the square of the difference between modelled m and GSTA observed values *o*:

$$\alpha = \sum_i^{\eta}(m - o)^2 \qquad \textbf{Equation S2}$$

With η the number of GSTA values (i.e. years) from 1880 to 2022 (η=143 years). For the purpose of fitting, the minimum value of GSTA was fixed to 0 by performing the following transformation:

GSTA*=GSTA-min(GSTA) **Equation S3**

The best fit was achieved for x_1=0.025, r=0.019 and K=11°C in 2400 (green logistic curve in Fig. S2, see also the inner panel). The other curves (the 9 curves in black) had α values that were slightly higher than the value of the green curve (Table S1). These curves should not be used as a likely projection of global temperatures, which are best investigated by means of Earth System Models (ESMs)(Masson-Delmotte et al. 2021). Although the 10 best curves were within the range of temperature changes documented for 2300 by the IPCC for moderate to high GHG emission scenarios (Medium Confidence, page 44)(Masson-Delmotte et al. 2021), this method was only applied to illustrate our theoretical approach. We chose the logistic curve that best fitted long-term changes in GSTA.

Modelling a cycle

Cyclical or pseudo-cyclical variability is a component of time series frequently observed (Chatfield 1996, Beaugrand 2019). We added a cyclical component C as follows:

$c=\gamma/2 \cos(\omega t + \varphi)$ **Equation S4**

With γ the amplitude (here γ=0.2°C), ω the angular frequency (i.e. ω affects the period of the cycle; here ω =0.5) and φ the phase at the origin (φ controls the phase of the oscillation at t = 0; here φ = 5) (Fig. S3a, black line). The angular frequency and the amplitude were chosen to be close to what was observed in GSTA (Fig. 1a-b). This cyclical variability can also be seen as a proxy for the alternation of negative and positive natural short-term perturbations.

Modelling year-to-year variability

High-frequency variability (here year-to-year variability) is a component always present in observed time series (Chatfield 1996, Beaugrand 2019). Here, this component (called hereafter component e) has a white noise of amplitude φ=0.5°C (Fig. S3a, orange line).

The cyclical and year-to-year variability were both added to the logistic curves.

Altering the amplitude of cyclical/year-to-year variability

Although rising autocorrelation and an increase in the variance are clear indicators of a system approaching a critical transition (Dakos et al. 2008), it is unclear what parameter may be used as an indicator of a system approaching a tipping point. The knowledge of the location of the tipping point is important because it indicates if changes remain reversible or not. Here, we propose that the variance of detrended GSTA (hereafter called dGSTA) may decrease when the system approaches a tipping point. Such a reduction in dGSTA variance is expected when a system approaches a tipping point because negative feedbacks remain at work to maintain the system inside its basin of attraction while strong external forces attempt to push it outside. This phenomenon should reduce

high-frequency variability. Therefore, we might expect positive perturbations to remain constant and negative ones to reduce because of a reduction in the strength of negative feedbacks also possibly associated with an increase in positive feedbacks.

To demonstrate this point, we altered the cycle (and the cycle + year-to-year variability) by modifying them in such a way that the negative part (i.e. cooling part) of the cycle diminishes as the system approaches a tipping point. (Note that in case of global cooling, the opposite would be true.) The cycles were altered as follows:

$$d_{t+1} = c_{t+1} + \theta(x_{t+1} - x_t + f_t) \quad \text{for all d>0} \quad \textbf{Equation S5}$$

$$d_{t+1} = c_{t+1} + (1-\theta)(x_{t+1} - x_t + f_t) \quad \text{for all d<0} \quad \textbf{Equation S6}$$

With d_{t+1} the altered cycle c_{t+1}, θ ($0 \leq \theta \leq 1$) the rate at which the positive part of the cycle c_t is altered and 1- θ the rate at which the negative part of the cycle is altered. When θ=0.5, the amplitude of the positive and negative parts of the cycle is equal at equilibrium (i.e. when f_t=0).

The changes in the cycles combined to year-to-year variability (c+e) were altered as follows:

$$g_{t+1} = (c_{t+1} + e_{t+1}) + \theta(x_{t+1} - x_t + f_t) \quad \text{for all d>0} \quad \textbf{Equation S7}$$

$$g_{t+1} = (c_{t+1} + e_{t+1}) + (1-\theta)(x_{t+1} - x_t + f_t) \quad \text{for all d<0} \quad \textbf{Equation S8}$$

With g_{t+1} the altered components "cycle + year-to-year variability" (i.e. c_{t+1} + e_{t+1}).

For all d>0, f_t the inertia parameter, is calculated as follows:

$$f_t = f_{t-1} + (x_{t+1} - x_t) - \theta(x_{t+1} - x_t)$$

After simplification, f_t becomes:

$$f_t = f_{t-1} + (1-\theta)(x_{t+1} - x_t) \quad \text{for all d>0} \quad \textbf{Equation S9}$$

For all d<0, f_t is calculated as follows:

$$f_t = f_{t-1} + (x_{t+1} - x_t) - (1-\theta)(x_{t+1} - x_t)$$

After simplification, f_t becomes:

$$f_t = f_{t-1} + \theta(x_{t+1} - x_t) \quad \text{for all d<0} \quad \textbf{Equation S10}$$

With f_1=0.

When d_t=0, no alteration of the cycle (and cycle + year-to-year variability) was performed.

To illustrate our approach, we modified the cycle (Supplementary Fig. 3a) by using Equations S5-6 (Fig. S3b and black curve in Fig. S3a) and the cycle + year-to-year variability by means of Equations S7-8 (Fig. S3c and orange curve in Fig. S3a). For both components (cycle and cycle/year-to-year variability), we arbitrarily chose θ=0.5 between t=1 and t=75 (Time Period 1 or TP1; equal amplitude of the negative and positive parts of the cycle), θ changed from 0.5 to 0.1 every step of 0.007 between t=76 and t=133 (TP2; the amplitude of the negative part of the cycle becomes progressively smaller than the positive part), θ=0.1 between t=134 and t=324 (TP3; the amplitude of the negative part of the cycle is smaller than the positive part), θ varies from 0.1 to 0.5 every step of 0.002 between t=325 and t=525 (TP4; the amplitude of the negative part of the cycle becomes progressively equal to that of the positive part), θ=0.5 between t=526 and t=601 (TP5; equal amplitude of the negative and positive parts of the cycle).

When θ=0.5 (TP1), the positive and negative parts of the cycle had the same amplitude. When θ changed from 0.5 to 0.1, the amplitude of the negative part of the cycle started to reduce progressively towards the end of TP3 when θ=0.1; the amplitude of the negative part of the cycle (and c + e) became smaller than the positive part. At TP4, θ changed from 0.1 to 0.5 and the amplitude once again equilibrated at the end of TP5 (Fig. S3); the delay between the alteration of θ and its result depends on f_t (Equations S9 and S10). In the main text, the cycle (and cycle + year-to-year variability) is termed altered cycle (or altered cycle + year-to-year variability).

Text S2

A first increase in GSTA also occurred during W1 (1910-1945, Fig. 1a and Fig. 2d). This was also preceded by a reduction in dGSTA variance (the period between yellow circles 1 and 2 in Fig. 2d) subsequently followed by an increase in autocorrelation and an increase in dGSTA variance (the period between yellow circles 2 and 3 in Fig. 2d). However, after a temporary reduction in dGSTA variance (the period between yellow circles 3 and 4), this indicator rose again and the autocorrelation fell (the period between yellow circles 4 and 5). The whole sequence was in general characterised by a much higher variability in the 30-year estimates of dGSTA variance and autocorrelation (Fig. 2d). In contrast to W1, the absence of variability in 30-year dGSTA variance and GSTA autocorrelation in W2 implies a strong directional change (Kump et al. 2004).

Supplementary Table

Table S1 | The combinations of x_1, r and K that best fits long-term changes (1880-2022) in GSTA. α: the sum of the square of the difference between modelled and GSTA values. X_1: GSTA at t=1. r: rapidity with which global temperature adjusts to new conditions. K: GSTA at the new dynamic equilibrium. These values should not be used as projections of global temperatures, which are best investigated by means of Earth System Models (ESMs)(Masson-Delmotte et al. 2021). This method was only applied to illustrate our theoretical approach in the section 2.2.

Best fit	α	X_1	r	K
1	**2.1855**	**0.025**	**0.0190**	**11**
2	2.1856	0.025	0.0190	12
3	2.1912	0.025	0.0190	13
4	2.1941	0.025	0.0190	10
5	2.2000	0.025	0.0190	14
6	2.2110	0.025	0.0190	15
7	2.2168	0.025	0.0190	9
8	2.2626	0.025	0.0190	8
9	2.3028	0.025	0.0200	4
10	2.3473	0.025	0.0190	7

Supplementary Figures

Figure S1 | Hypothetical changes in global temperature using a family of logistic curves with different values of global temperature at equilibrium (a) and different speeds of temperature changes (b). In **a**, from low to high global temperature, K=2, 4, 6, 8 and 10°C with r=0.05 and x_1=0.025°C (Equation 1). In **b**, from left to right: r=0.6, 0.2, 0.1, 0.05 and 0.04°C for K=3°C and x_1=0.025°C. A state is defined as a dynamic equilibrium (also called a basin of attraction). It can therefore exhibit some variability, be cyclical or include year-to-year variability. Here, we assume that the tipping point is where the increase in global temperature becomes noticeable. Note that the critical transition can be very rapid in some cases, corresponding to a stepwise shift (left curve in panel **b**). In other cases, the shifts may take several decades to centuries (right curves in panel **b**). A more precise characterisation of the different phases is given in Figure S4. No cycle or year-to-year variability is included here. See Text S1.

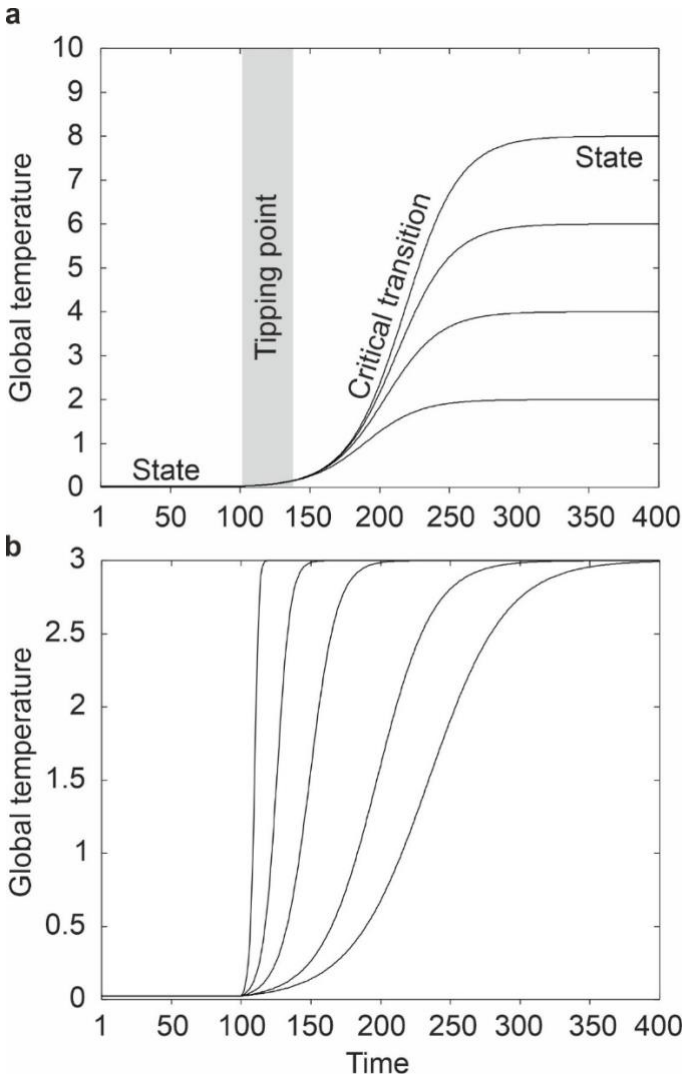

Figure S2 | Logistic curves that fit best long-term changes in observed GSTA. A total of 63105 combinations of parameters was used. The best ten curves are shown: the best fit is in green and, the others in black. The GSTA time series (1880-2022) is superimposed on top in red. The inner panel shows the relationship between the best simulated logistic curve (black) and GSTA (red). These curves should not be used as projections of global temperatures, which are best investigated by means of Earth System Models (Masson-Delmotte et al. 2021). This method was only applied to illustrate our theoretical approach in the Methods section (see Text S1).

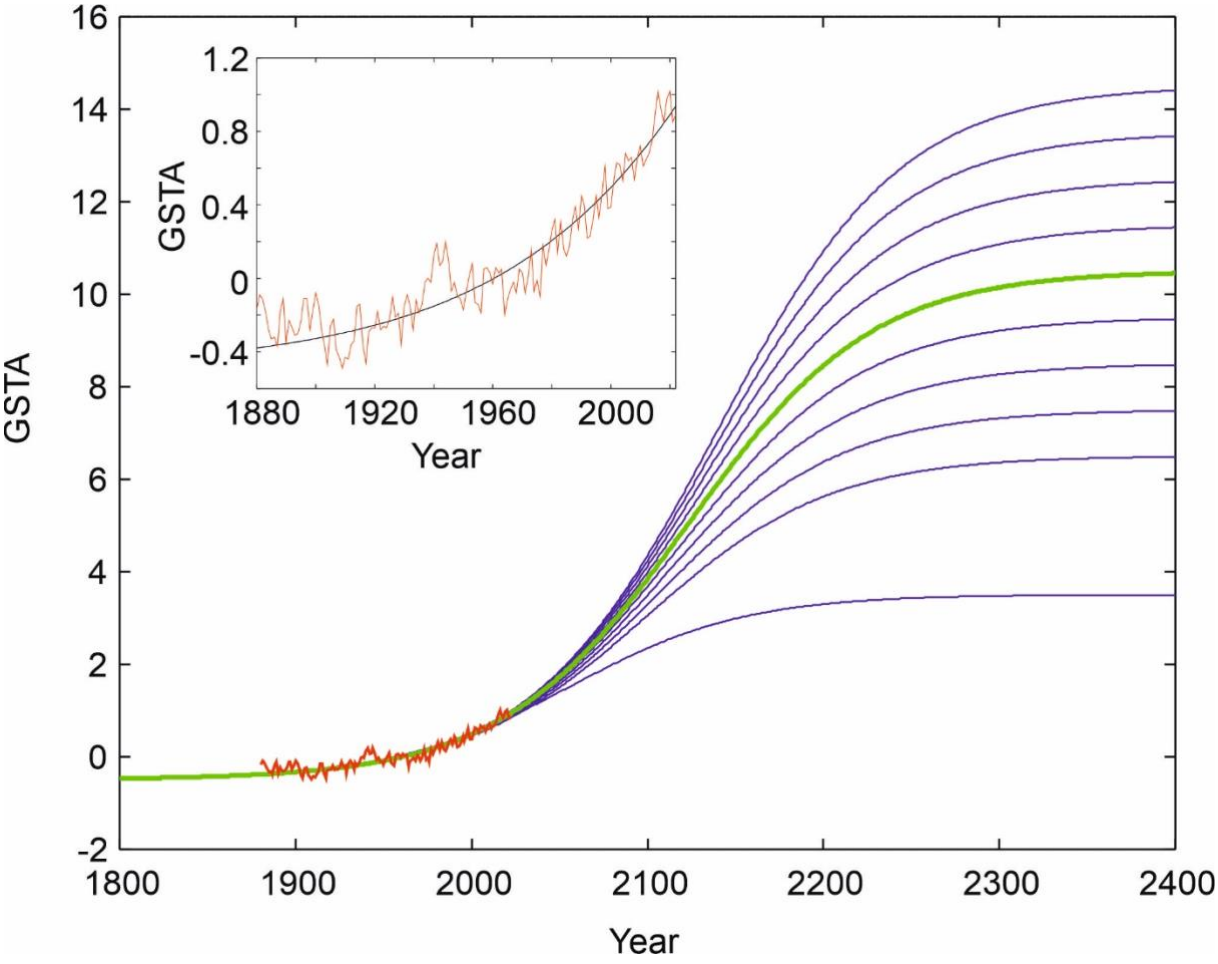

Figure S3 | Hypothetical cyclical variability from 1800 to 2400 without and with year-to-year variability and alteration of the negative and positive parts of the cycle. (**a**) Unaltered cycle without (black) and with (orange) year-to-year variability. (**b**) Altered negative and positive parts of the cycle. Time period 1 (TP1): the amplitudes of positive and negative phases are equal (1800-1874); TP2: the amplitude of negative phases become progressively lower than positive phases, the latter remaining unchanged (1875-1932); TP3: negative phases are smaller than positive ones (1933-2123); TP4: the amplitude of negative phases become progressively higher to equal the positive phases at the end (2124-2324); TP5: positive and negative phases have an equal amplitude (2325-2400). (**c)** The alteration of the negative and positive part of the cycle is similar to (**b**) but a year-to-year variability was added to the cyclical variability (see panel **a** in orange). See Text S1 and Section 2.2.

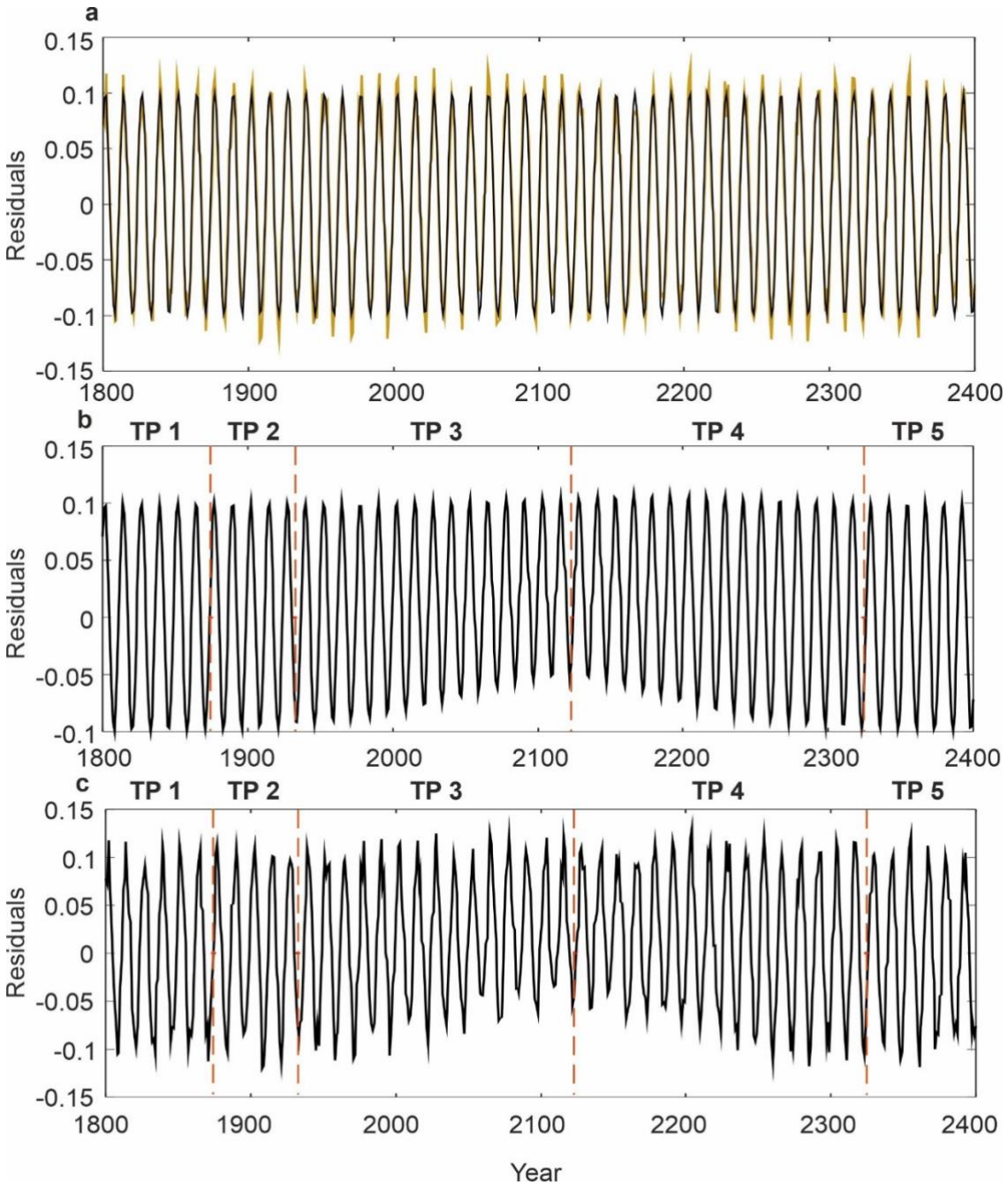

Figure S4 | Multiscale variability analysis on simulated changes in global temperature (1800-2400). **a-c** Changes in global temperature as simulated by a logistic curve and a cycle. **d-f** Changes in global temperature as simulated by a logistic curve, a cycle and year-to-year variability (Section 2.2 and Text S1). The cycle (and the cycle + year-to-year variability) were altered according to Equations S5-8 (Text S1) to simulate a reduction in the negative phases of the cycle triggered by an assumed reduction in negative feedbacks or an increase in positive feedbacks when the system approaches a tipping point (Text S1). **a,d** Comparison of our simulated changes in global temperature (black) with GSTA (red). For visualisation purposes, we subtracted our simulated time series by the difference between the average of the simulated and the observed (GSTA) time series for 1880-2022. Note that differences between panels b and e are minor. The differences can be better seen on panels **a** and **d**. **b,e** Long-term changes in global temperature without **(b)** and with **(e)** year-to-year variability. **c,f** Multiscale variability analysis (time windows from 1 to 15 years) in simulated global temperature without **(c)** and with **(f)** year-to-year variability. See Text S1.

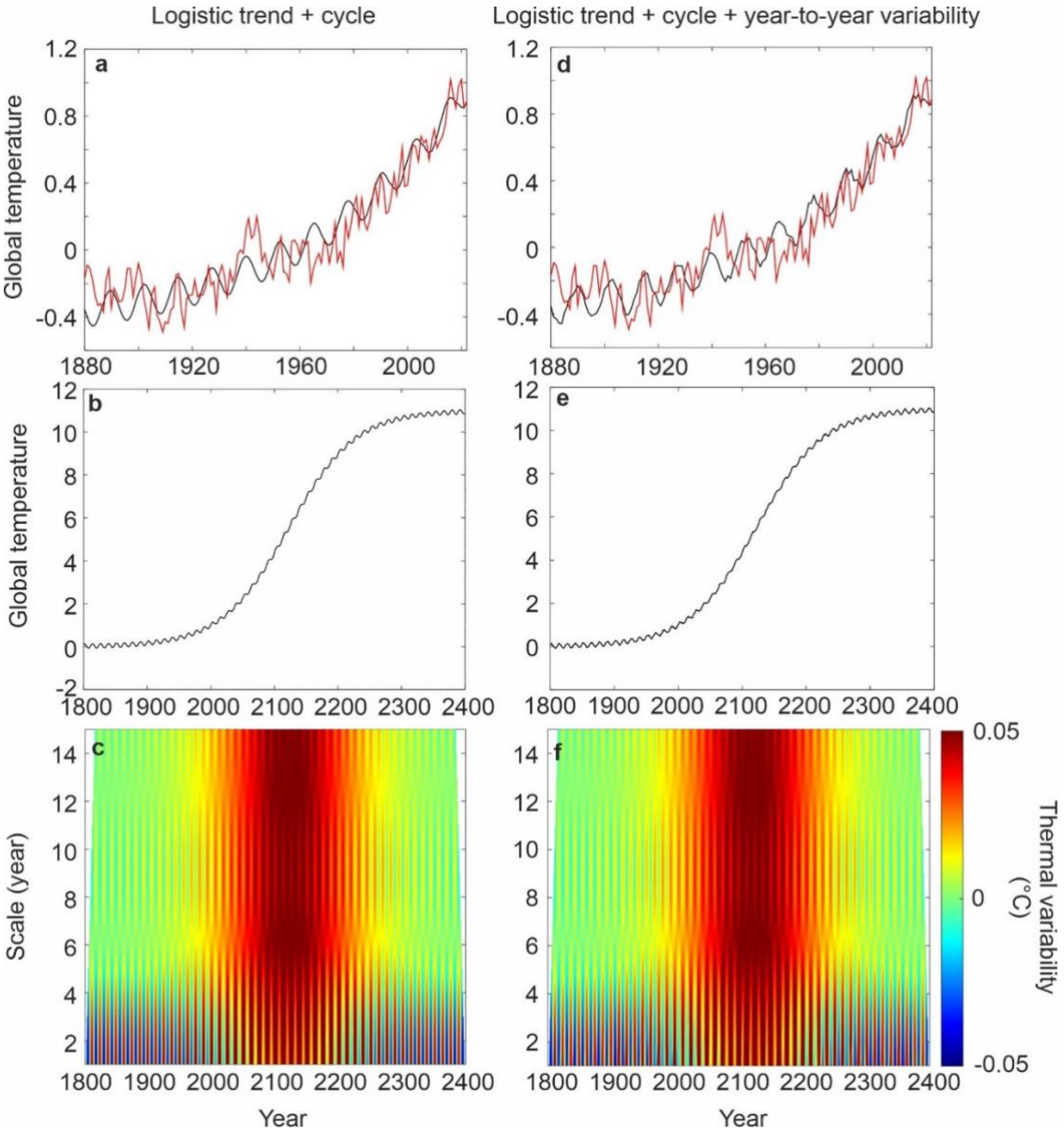

Figure S5 | Long-term changes in variance, autocorrelation and trend of simulated global temperature from 1800 to 2400. (**a-b**) variance assessed on detrended simulated global temperature (similar to detrended GSTA or dGSTA variance), (**a**) variance on the altered cycle (time series shown in Supplementary Fig. 3b) and (**b**) variance on the cycle and year-to-year variability (time series shown in Fig. S3c), (**c**) Autocorrelation and (**d**) Trend (°C per decade) on all three components (trend + cycle + year-to-year variability) and (**e**) **H** Number of years needed for the trend to reach the maximum amplitude of detrended simulated global temperature (time series shown in Fig. S4e). HFV in H: high-frequency variability in H. No SSA was performed in this case in contrast to the observed GSTA (see Figure 1); such a SSA was not needed here because we worked on simulated time series. Detrended global temperature was therefore simulated global temperature, i.e. a cycle without (**a**) and with (**b**) year-to-year variability (therefore both without the logistic trend). The cycle (and the cycle + year-to-year variability) were altered according to Equations S5-8 (Text S1) to simulate a reduction in the negative phases of the cycle triggered by an assumed reduction in negative feedbacks (associated or not to an increase in positive feedbacks) when the system approaches a tipping point (Text S1). All variables were calculated for each 30-year period from 1800 (end year: 1829) to 2371 (end year: 2400). Five orders of autocorrelation are indicated from order-1 (lag of one year, green) to order-2-4 (lags of 2-4 years, black) and order-5 (lag of 5 years, red). The vertical dashed lines denote the instability points (left and right) and the inflection point (middle). The critical transition is assumed to be located between the left and right vertical dashed lines. See Text S1.

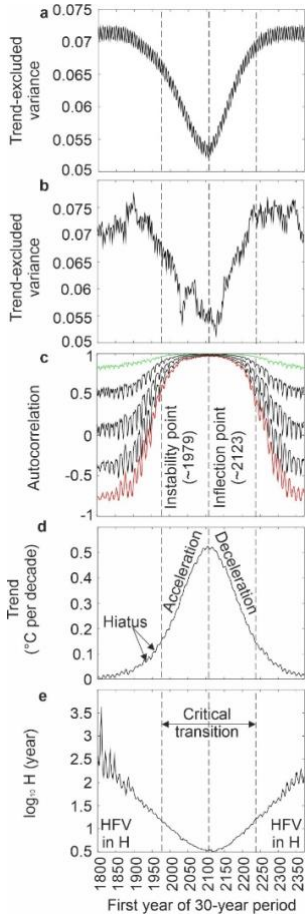

Figure S6 | 30-year mean (order 1-5) autocorrelation of the simulated global temperatures (trend + altered cycle and year-to-year variability) *versus* 30-year trend-excluded (altered cycle + year-to-year variability) variance. All variables were calculated for each 30-year period from 1880 (end year: 1909) to 2371 (end year: 2400) on the simulated global temperatures seen in Fig. S4e. Clockwise, the five periods of alteration in the amplitude of the negative parts of the cycle are indicated by a colour (see legend on the figure). 1800-1874: θ=0.5 (i.e. equal amplitude of the negative and positive parts of the cycle); 1875-1932: from θ=0.5 to 0.1, every step of 0.007; 1933-2123: θ=0.1 (i.e. low amplitude of the negative parts with respect to the positive parts of the cycle); 2124-2324: θ=0.1 to 0.5 every step of 0.002; 2325-2400: θ=0.5. This figure should be compared with Fig. 2d. See Text S1.

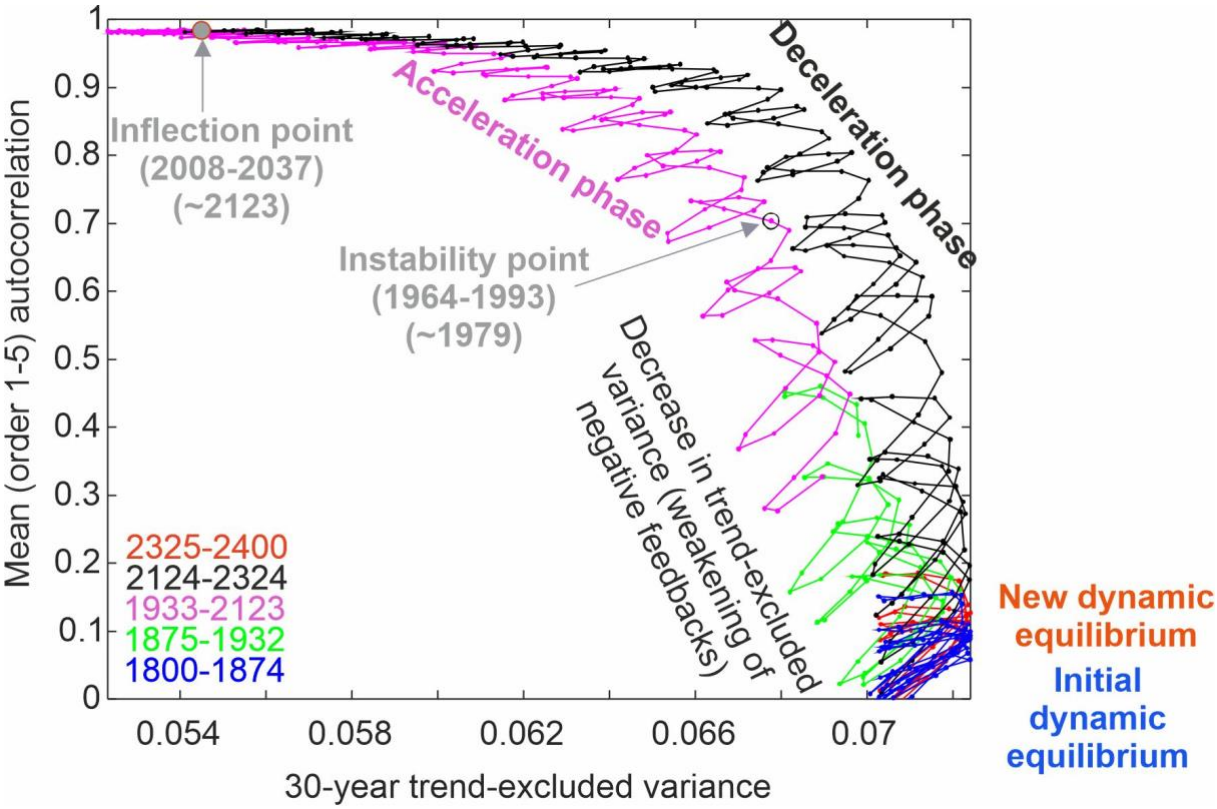

References

Beaugrand G (2019) Predictions of unprecedented biological shifts in the global ocean. The Marine Biologist 13:6-7

Beaugrand G, Balembois A, Kléparski L, Kirby RR (2022) Addressing the dichotomy of fishing and climate in fishery management with the FishClim model. Communications Biology 5:1146

Chatfield C (1996) The analysis of time series: an introduction, Vol. Chapman and Hall, London

Dakos V, Scheffer M, van Nes EH, Brovkin V, Petoukhov V, Held H (2008) Slowing down as an early warning signal for abrupt climate change. Proceedings of the National Academy of Sciences of the United States of America 105:14308–14312

Kump LR, Kasting JF, Crane RG (2004) The Earth system, Vol. Pearson Prentice Hall, Upper Saddle River, NJ

Masson-Delmotte V, Zhai P, Pirani A, Connors SL, Péan C, Berger S, Caud N, Chen Y, Goldfarb L, Gomis MI, Huang M, Leitzell K, Lonnoy E, Matthews JBR, Maycock TK, Waterfield T, Yelekçi O, Yu R, Zhou B (2021) Climate Change 2021: The Physical Science Basis. Contribution of Working Group I to the Sixth Assessment Report of the Intergovernmental Panel on Climate Change Vol. Cambridge University Press, Cambridge